Journal of Alloys and Compounds 588 (2014) 633–637

Contents lists available at ScienceDirect

Journal of Alloys and Compounds

journal homepage: www.elsevier.com/locate/jalcom

Structural stability of diffusion barriers in thermoelectric SbTe: From first-principles calculations to experimental results

Hsiao-Hsuan Hsu [a,b], Chun-Hu Cheng [c,*], Shan-Haw Chiou [d], Chiung-Hui Huang [d], Chia-Mei Liu [a], Yu-Li Lin [a], Wen-Hsuan Chao [d], Ping-Hsing Yang [d], Chun-Yen Chang [b], Chin-Pao Cheng [c,*]

[a] *Green Energy and Environment Research Lab., Industrial Technology Research Institute, Hsinchu 31040, Taiwan, ROC*
[b] *Department of Electronics Engineering, National Chiao Tung University, Hsinchu 30010, Taiwan, ROC*
[c] *Department of Mechatronic Technology, National Taiwan Normal University, Taipei 10610, Taiwan, ROC*
[d] *Material and Chemical Research Lab., Industrial Technology Research Institute, Hsinchu 31040, Taiwan, ROC*

A R T I C L E I N F O

Article history:
Received 19 September 2013
Received in revised form 17 November 2013
Accepted 21 November 2013
Available online 28 November 2013

Keywords:
Thermoelectric device
Diffusion barrier
SbTe
First-principles calculations

A B S T R A C T

This study involved developing robust diffusion barrier for *n*-type antimony telluride (SbTe) thermoelectric devices. Compared to conventional Ni barrier, the mid-band metals of Ta and TaN with favored ohmic-like contact exhibited smaller diffusion tail because of structurally stable interface on SbTe, which have been supported by first-principles calculations and demonstrated by experimental results. Furthermore, the TaN barrier has strong ionic Ta–N bonding and a high total energy of −4.7 eV/atom that could effectively suppress the formation of SbTe-compounds interfacial layer.

© 2013 Elsevier B.V. All rights reserved.

1. Introduction

Thermoelectric devices were used for direct energy conversion between heat and electricity because of their unique properties, including free-moving parts, no requirement for refrigerants, and high reliability [1,2]. The thermoelectric devices consisted of copper electrodes, solder layers, diffusion barriers, and thermoelectric materials. The efficiency of the thermoelectric devices was evaluated according to a dimensionless figure of merit, $ZT = (S^2\sigma T/\kappa)$, where S refers to Seebeck coefficient, σ to electrical conductivity, T to absolute temperature, and κ to thermal conductivity [3]. Considering the superior thermoelectric characteristics near room temperature with $ZT \sim 1$, semiconducting thermoelectric materials, such as bismuth telluride (Bi_2Te_3) and antimony telluride (Sb_2Te_3) compounds were used on the applications of solid-state cooling and power generation [4,5]. However, the inter-diffusion problem caused by the soldering process appeared to deteriorate the thermoelectric properties because of a CuTe formation [6] and carrier concentration change [7,8], which must be solved. Consequently, various diffusion barriers, such as TiWN [9], Ti/Au [10], $Ta_{40}Si_{14}N_{46}$ [6], TiW/Au [11], and Sb [12], were proposed as a solution, except for commercial Ni diffusion barrier. However, a thorough understanding of interface diffusion mechanisms is required.

In this study, the metal-nitride TaN and Ta (with a high melting point and thermal stability) were proposed to serve as diffusion barriers to further stabilize interface reactions. The Ta and TaN barriers have been used to block Cu diffusion in the CMOS backend interconnect process at 400 °C [13]. Moreover, the interface diffusion behavior was also investigated in detail based on theoretical simulations, leakage conduction mechanism, and material structure analysis.

2. Experimental procedures

The 1-μm-thick SbTe films were deposited using a multi-chamber sputter system with a processing temperature of 130 °C on a 1-μm-thick SiO_2 grown on a Si substrate. Prior to the deposition process, the chamber was evacuated at a base pressure of 3×10^{-6} Torr, and during the deposition process, the pressure was maintained at 5×10^{-3} Torr. After the film deposition, in situ annealing under argon atmosphere at 250 °C for 30 min was performed to enhance film quality. Subsequently, metal depositions of 100-nm-thick Ni, Ta, and TaN serving as diffusion barrier layers were performed. The TaN film was deposited under an argon ambient (100 sccm) with 10% N_2 mixing (10 sccm) and a chamber pressure of 5 mTorr at a dc power of 800 W. Next, post-deposition annealing (PDA) at 200 °C close to the soldering temperature in the thermoelectric module was applied to all devices. To analyze the carrier transport mechanism at the interface, a low-temperature measurement for various junction diffusion barriers on a *p*-type Si substrate was conducted. SbTe-based thermoelectric materials are known to exhibit native antisite defects in which excess Te atoms occupy Sb lattice sites and behave similarly to *n*-type conductions [14], which is consistent with our Te/Sb composition ratio

* Corresponding authors. Tel.: +886 2 23583074.
E-mail addresses: chcheng@ntnu.edu.tw (C.-H. Cheng), cpcheng@ntnu.edu.tw (C.-P. Cheng).

0925-8388/$ - see front matter © 2013 Elsevier B.V. All rights reserved.
http://dx.doi.org/10.1016/j.jallcom.2013.11.138

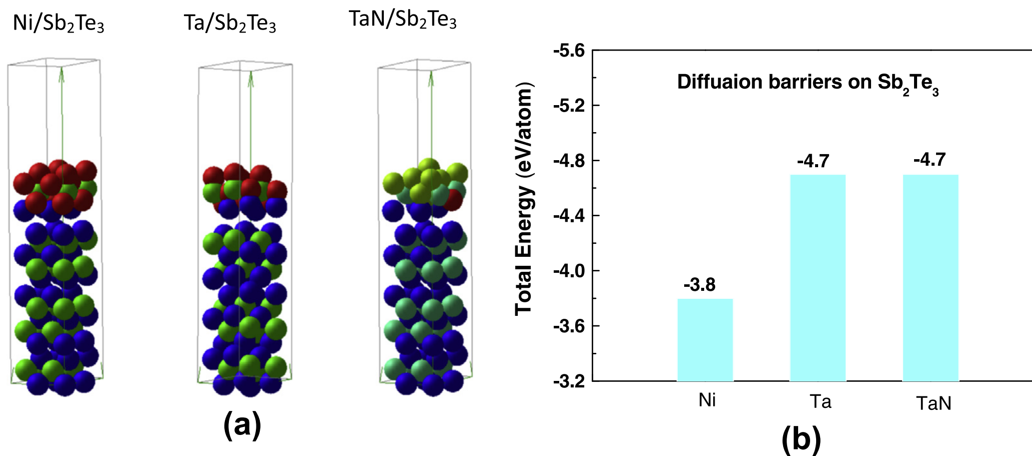

Fig. 1. Relaxed atomic structures of (a) Ni, Ta, and TaN diffusion barriers on Sb_2Te_3 thermoelectric. (b) The total energies of Ni, Ta, and TaN diffusion barriers in contact with Sb_2Te_3 thermoelectric.

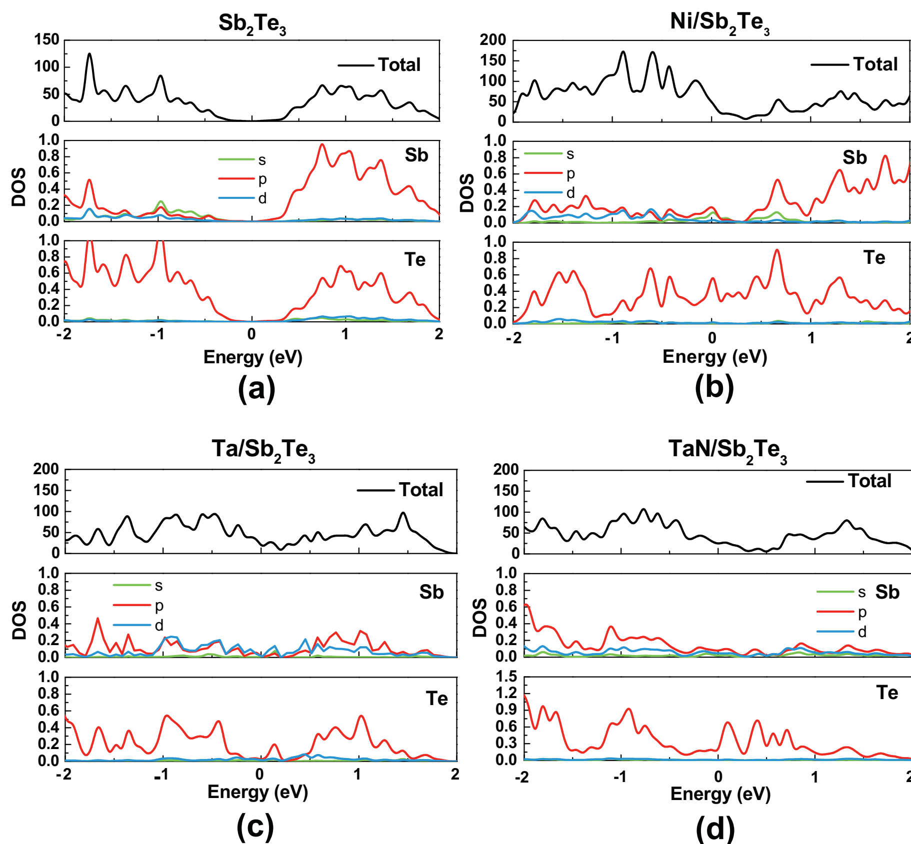

Fig. 2. Total and partial density of states of (a) Sb_2Te_3 bulk and (b) Ni/Sb_2Te_3, (c) Ta/Sb_2Te_3, and (d) TaN/Sb_2Te_3 interfaces.

of 1.8 implemented using energy dispersive X-ray spectrometry (EDX). The electrical characteristics were measured using a HP4156C semiconductor parameter analyzer. These samples were inspected using grazing incidence X-ray diffraction (GIXRD), EDX, and high-resolution transmission electron microscopy (HRTEM). The self-consistent *ab initio* calculations were also performed to evaluate the lowest energy for interfacial structure to support our experimental results.

3. Results and discussion

To analyze the thermal dynamic stability of the interface, the total energy was calculated by relaxing the $2 \times 2 \times 1$ supercell with constrained Sb_2Te_3, where the unit cell was found to contain six Sb atoms and nine Te atoms. One-third of the Te atoms were surrounded by six Sb atoms, whereas two-thirds of the Te atoms were surrounded by three Sb atoms. The Sb_2Te_3 crystals exhibited a hexagonal structure. The calculated lattice constant of an *a*- and *c*-axis were equal to 4.264 Å and 30.428 Å, respectively. Fig. 1a illustrates the relaxed atomic structure of Sb_2Te_3 in contact with Ni, Ta, and TaN diffusion barriers. The interfaces were formed by Ni–Sb, Ta(N)–Sb, Ni–Te, and Ta(N)–Te bonds. The interfaces were modeled using a superlattice, including one interface and a 17 Å vacuum layer separating the periodic images along the *c*-axis.

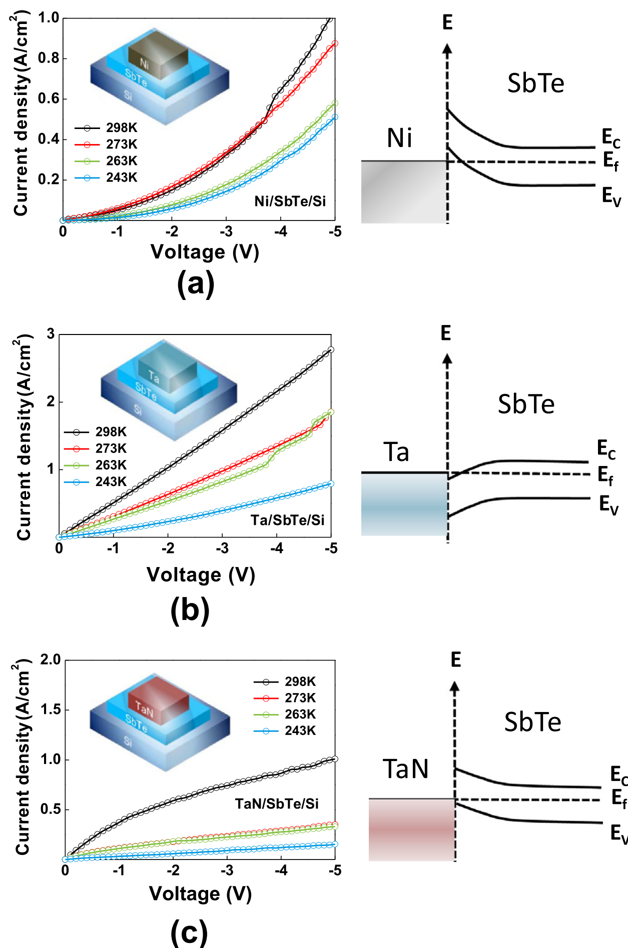

Fig. 3. The current–voltage characteristics measured from 243 K to 298 K, and energy band diagrams of (a) Ni/SbTe, (b) Ta/SbTe, and (c) TaN/SbTe junctions. The insets this figure are the schematic structures of metal–semiconductor junctions.

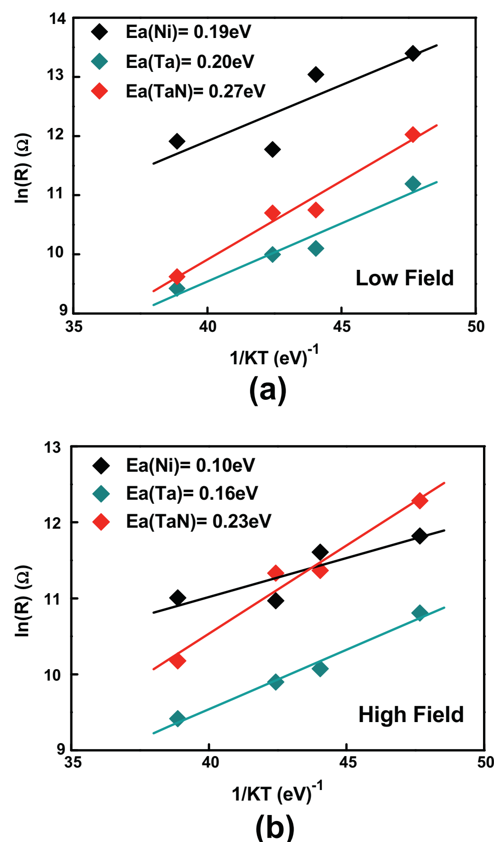

Fig. 4. The fitting curves of *ln* (*R*) verse of 1/*KT* for Ni/SbTe, Ta/SbTe, and TaN/SbTe junctions at (a) low and (b) high electric field.

Subsequently, the first-principles calculations were performed using density-functional theory (DFT) within the self-consistent total-energy plane-wave basis code VASP (Vienna *ab Initio* Simulation Package) [15,16]. The interaction between atomic cores and electrons was demonstrated using the projector-augmented-wave (PAW) method, using s, p, and d waves inside all atomic spheres. The exchange–correlation energy was approximated using the generalized gradient approximation (GGA). As presented in Fig. 1b, the total energy of −4.7 eV/atom for the TaN/Sb_2Te_3 system appeared to be lower than that of −3.8 eV/atom for the Ni/Sb_2Te_3 interface, indicating that TaN contact with Sb_2Te_3 is a favorable structure. Thus, Ta/Sb_2Te_3 and TaN/Sb_2Te_3 systems featured similar thermodynamic stability at the Sb_2Te_3 interface.

The density of states (DOS) of Sb_2Te_3, Ni/Sb_2Te_3, Ta/Sb_2Te_3, and TaN/Sb_2Te_3 film structures are illustrated in Fig. 2a–d, respectively. All of the angular momentum projections (s, p, and d) on all of the atoms were performed to yield a partial density of states (PDOS). The Fermi energy aligned with zero depended on the interfacial bonding configuration. The calculated energy band gap of 0.31 eV, presented in Fig. 2a, was preferred to semiconducting properties, which was consistent with experimental results [14]. The slopes for both conduction-band minimum (CBM) and valence-band maximum (VBM) of Sb_2Te_3 were responsible for a Seebeck effect in the thermoelectric Sb_2Te_3. After the diffusion barriers were in contact with Sb_2Te_3, the DOS became gapless and connected between the CBM and the VBM. The Te PDOS near the Fermi energy were mainly attributed to the p-orbital at three barrier/Sb_2Te_3 interfaces. The Sb PDOS near the Fermi energy were ascribed to both p- and d-orbitals at the Ta/Sb_2Te_3 and TaN/Sb_2Te_3 interfaces, whereas the p-orbital near CBM dominated the PDOS at the Ni/Sb_2Te_3 interface. In Fig. 2b, the Sb PDOS curve at the Ni/Sb_2Te_3 interface is significantly high at the CBM, implying the contribution of carrier concentration on *n*-type feature. The Sb PDOS at the Ta/Sb_2Te_3 interface is a homogenous distribution and resembles the Sb PDOS curve at the TaN/Sb_2Te_3 interface, as illustrated in Fig. 2c and d. The similarity of electronic structures between Ta/Sb_2Te_3 and TaN/Sb_2Te_3 interfaces may explain the similar total energy.

Fig. 3 presents the current–voltage (*I*–*V*) characteristics of barrier/SbTe junctions at various temperature ranges from 243 K to 298 K. The schematic plots of the device structure are presented in the insets of Fig. 3. The expected work functions of Ni, Ta, and TaN corresponded to the values of 5.1 [17], 4.25 [18], and 4.4 [19] eV, respectively. To investigate the conduction mechanism precisely, the energetic electron transport at the junction interface was evaluated at low temperature. According to the measured results, the Schottky rectifying effect was observed at the Ni/SbTe interface. The Ni barrier with high work function easily formed a high barrier height for Schottky conduction after band alignment, which could degrade thermoelectric energy transport. By contrast, Ta/SbTe and TaN/SbTe were preferred to form ohmic-like conductions because Ta and TaN belonged to mid-band metals with lower work functions than those of the Ni barrier, which was suitable for both *n*- and *p*-type thermoelectric materials with a narrow band gap of only 0.3 eV. In addition, the increased current densities with temperature were characterized by a negative temperature coefficient, indicating that the electron conduction in SbTe was semiconducting.

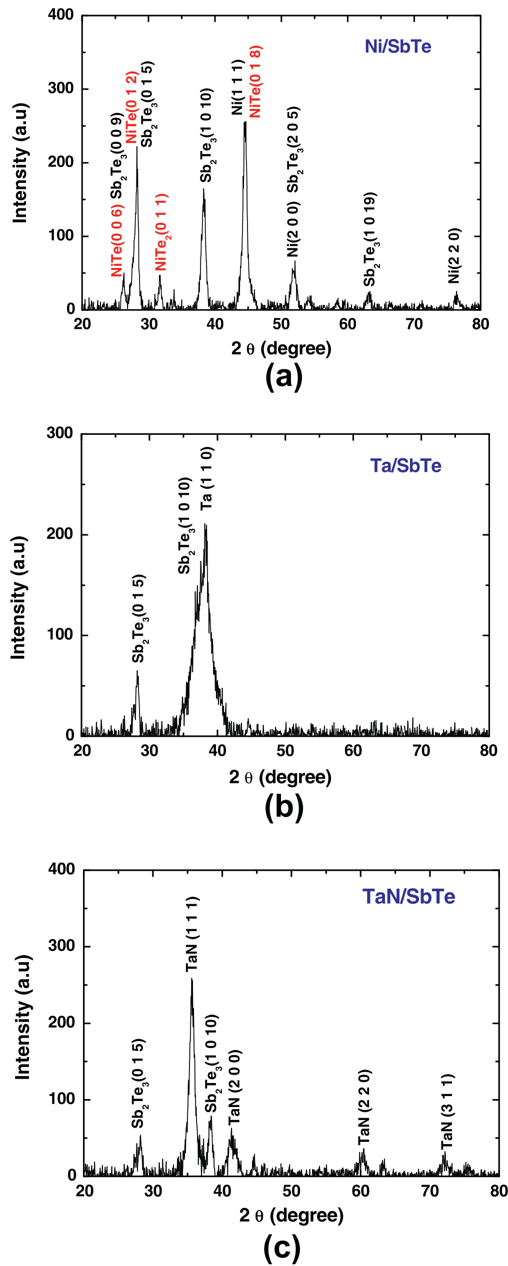

Fig. 5. GIXRD spectra of (a) Ni/SbTe, (b) Ta/SbTe, and (c) TaN/SbTe interfaces after 200 °C PDA treatment.

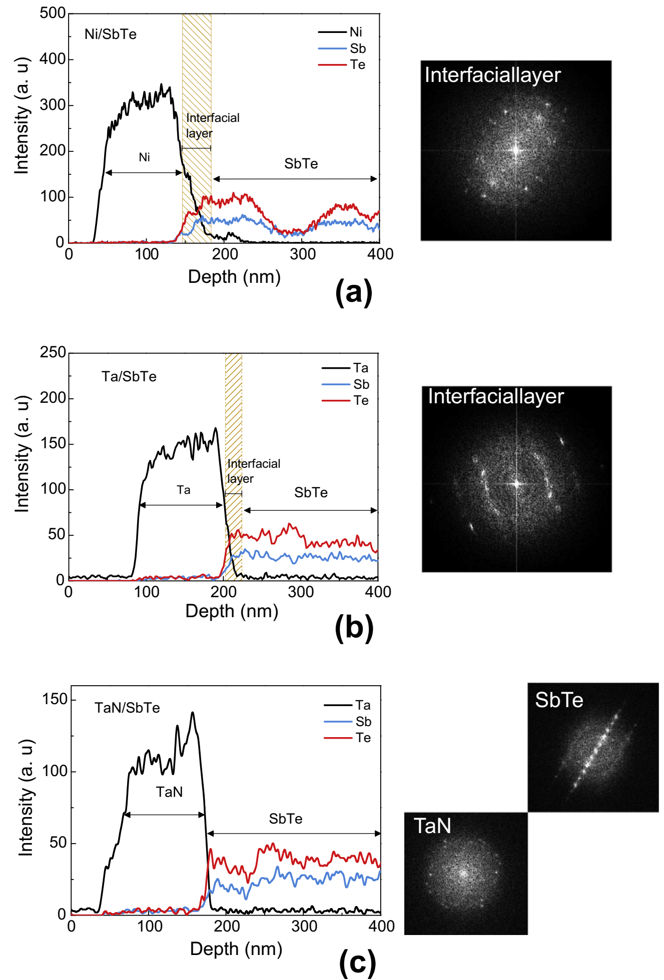

Fig. 6. EDX depth profiles and FFT patterns of (a) Ni/SbTe, (b) Ta/SbTe, and (c) TaN/SbTe interfaces after 200 °C PDA.

Fig. 4 presents the Arrhenius plots of ln (R) versus $1/KT$ for Ni/SbTe, Ta/SbTe, and TaN/SbTe junctions at low and high electric fields, where R is the electrical resistance, K is the Boltzmann constant, and T is the absolute temperature. The electrical resistance dependence of the measured temperature can be described using the following equation:

$$R = R_0 \, exp\left(\frac{E_a}{KT}\right) \tag{1}$$

Here, R_0 is the pre-exponential factor and E_a is the activation energy. The E_a associated with interface states were extracted at the slope of each linear curve. These linear Arrhenius plots were dependent on measured temperature and applied bias, suggesting that related carrier transport was mainly attributed to thermally-activated hopping conduction [20,21]. In a low electric field of Fig. 4a, the extracted E_a for Ni, Ta, and TaN metal contacts were 0.19, 0.20, and 0.27 eV, respectively. In Fig. 4b, the extracted E_a values at a high electric field showed similar tendency, but were lower than those of low electric field. The energy difference between low and high electric field can be ascribed to phonon scattering in a high field, thus affecting the carrier transport and lowering E_a. The high E_a implies that the low-resistance ohmic-like conduction was stable enough to be maintained at high temperature. This is important for thermoelectric efficiency because electron transport should be affected by interface energetic barrier with temperature dependence.

To verify the blocking effect of diffusion barriers and thermoelectric atoms (Sb and Te), a 200 °C PDA was performed on stacked structures of barriers/SbTe/SiO_2/Si. Fig. 5a–c presents the GIXRD patterns of the Ni/SbTe, Ta/SbTe, and TaN/SbTe interfaces. The peaks of (011), (006), (018), and (012) assigned to the NiTe and $NiTe_2$ phases confirmed atomic inter-diffusion near the Ni/SbTe interface because of Te out-diffusion, even with the temperature as low as 200 °C. The out-diffusion of Te could increase the possibility of the Te site occupied by Sb, and thereby, create more vacancies in SbTe that strongly drive the occurrence of inter-diffusion behavior between Ni and SbTe. However, no apparent SbTe-related-alloy formation is observed in Ta/SbTe and TaN/SbTe interfaces, indicating that Ta and TaN barrier have good barrier property to block the out-diffusion of Sb and Te atoms.

To further investigate the inter-diffusion effect, the EDX was performed to observe depth profiles of various barriers at SbTe interfaces after 200 °C PDA. The intermetallic diffusion behaviors

at various barriers/SbTe interfaces were also confirmed using Fast Fourier Transform (FFT). The EDX depth profile in Fig. 6a indicates a 90-nm-thick interfacial layer observed at the Ni/SbTe interface. This resulted from the Te atom possessing a considerably high vapor pressure that is highly sensitive to process temperature and causes a long diffusion profile tail. The Te out-diffusion changed the atomic ratio of SbTe and also degraded the thermoelectric properties. However, a narrow interfacial layer at the Ta/SbTe interface suggests that the Ta barrier presented an adequate blocking capability for Sb and Te, but could not effectively improve atom diffusion behavior, as presented in Fig. 6b. By contrast, a sharp interface profile was differentiated at the TaN/SbTe interface (Fig. 6c), which suggests that the atomic diffusion behavior was further suppressed by a diffusion barrier of a TaN metal with strong Ta–N bonding. The formation of strong ionic bonding (Ta–N) was considerably more stable than a pure Ta barrier. The metal barriers with nitrogen incorporation, such as TaN and TiN, exhibited more enhanced high-temperature thermal stability than the pure metals that were proved in the CMOS backend process [13]. Thus, replacing Ni with metal-nitride TaN could effectively suppress the formation of interfacial layer with SbTe-compounds and substantially improve the out-diffusion of SbTe bulk at a soldering temperature.

4. Conclusion

In conclusion, we used mid-band metals of Ta and TaN as diffusion barriers to improve the inter-diffusion between diffusion barriers and thermoelectric SbTe materials. Compared with conventional Ni barriers, the Ta exhibited a smaller diffusion tail because of small total energy and stable surface bonding. Notably, the TaN barrier with strong ionic bonding (Ta–N) and a high total energy of −4.7 eV/atom in contact with thermoelectric SbTe demonstrated adequate thermal stability to alleviate the diffusion behavior that originated from unstable Te-based SbTe thermoelectric materials. Related results and discussions were demonstrated using experimental comparisons and theoretical simulations by using first-principles calculations.

Acknowledgments

The authors are grateful to the Bureau of Energy, Ministry of Economic Affairs, Taiwan, ROC and the National Science Council (NSC) of Taiwan, ROC, for the financial support.

References

[1] F.J. DiSalvo, Science 285 (1999) 703–706.
[2] Y. Lan, A.J. Minnich, G. Chen, Z. Ren, Adv. Funct. Mater. 20 (2010) 357–376.
[3] S.S. Kim, F. Yin, Y. Kagawa, J. Alloys Comp. 419 (2006) 306–311.
[4] A. Majumdar, Science 303 (2004) 777–778.
[5] E. Koukarenko, G.P. Vassilev, N. Nancheva, P. Docheva, J.C. Tedenac, N. Freti, V. Shepelevich, J. Alloys Comp. 287 (1999) 239–242.
[6] T. Kacsich, E. Kolawa, J.P. Fleurial, T. Caillat, M.-A. Nicolet, J. Phys. D: Appl. Phys. 31 (1998) 2406–2411.
[7] Y.C. Lan, D.Z. Wang, G. Chen, Z.F. Ren, Appl. Phys. Lett. 92 (2008) 101910.
[8] J. Bludska, S. Karamazov, J. Navratil, I. Jakubec, J. Horak, Solid State Ionics 171 (2004) 251–259.
[9] G. Zeng, J.H. Bahk, J.E. Bowers, H. Lu, A.C. Gossard, S.L. Singer, A. Majumdar, Z. Bian, M. Zebarjadi, A. Shakouri, Appl. Phys. Lett. 95 (2009) 083503.
[10] W.P. Lin, D.E. Wesolowski, C.C. Lee, J. Mater. Sci.: Mater. Electron. 22 (2011) 1313–1320.
[11] W.P. Lin, C.C. Lee, IEEE Trans. Compon. Pack. Manuf. Technol. 1 (2011) 1311–1318.
[12] F. Li, X. Huang, W. Jiang, L. Chen, AIP Conf. Proc. 1449 (2012) 458–462.
[13] S.C. Sun, M.H. Tsai, C.E. Tsai, H.T. Chiu, Symp. VLSI Technol. Dig. Tech. Pap. (1995) 29–30.
[14] Y. Kim, A. DiVenere, G.K.L. Wong, J.B. Ketterson, S. Cho, J.R. Meyer, J. Appl. Phys. 91 (2002) 715–718.
[15] G. Kresse, J. Joubert, Phys. Rev. B59 (1999) 1758–1775.
[16] G. Kresse, J. Furthmuller, Comput. Mater. Sci. 6 (1996) 15–50.
[17] C.H. Cheng, A. Chin, F.S. Yeh, IEEE Electron. Dev. Lett. 31 (2010) 1020–1022.
[18] R.G. Wilson, J. Appl. Phys. 37 (1966) 3170–3172.
[19] H.Y. Yu, C. Ren, Y.C. Yeo, J.F. Kang, X.P. Wang, H.H.H. Ma, M.F. Li, D.S.H. Chan, D.L. Kwong, IEEE Electron. Dev. Lett. 25 (2004) 337–339.
[20] S. Espevik, C.H. Wo, R.H. Bube, J. Appl. Phys. 42 (1971) 3513–3529.
[21] F. Briones, D. Gaimayo, C. Ortiz, Thin Solid Films 78 (1981) 385–395.